

# Spectroscopy of the heaviest nuclei (theory)

**A. V. Afanasjev and H. Abusara**

Department of Physics and Astronomy, Mississippi State University, Mississippi State,  
Mississippi 39762, USA

**E. Litvinova**

GSI Helmholtzzentrum für Schwerionenforschung, D-64291 Darmstadt, Germany  
Institut für Theoretische Physik, Goethe-Universität, D-60438 Frankfurt am Main, Germany

**P. Ring**

Physik-Department der Technischen Universität München, D-85748 Garching, Germany

E-mail: [afanasjev@erc.msstate.edu](mailto:afanasjev@erc.msstate.edu)

**Abstract.** Recent progress in the applications of covariant density functional theory (CDFT) to the description of the spectroscopy of the heaviest nuclei is reviewed. The analysis of quasiparticle spectra in actinides and the heaviest  $A \sim 250$  nuclei provides a measure of the accuracy of the description of single-particle energies in CDFT and an additional constraint for the choice of effective interactions for the description of superheavy nuclei. The response of these nuclei to the rotation is rather well described by cranked relativistic Hartree+Bogoliubov theory and it serves as a supplementary tool in configuration assignment in odd-mass nuclei. A systematic analysis of the fission barriers with allowance for triaxial deformation shows that covariant density functional theory is able to describe fission barriers on a level of accuracy comparable with the best phenomenological macroscopic+microscopic approaches.

## 1. Introduction

The study of the nuclei around  $^{254}\text{No}$ , the heaviest elements for which detailed spectroscopic data can be obtained with the current generation of facilities [1], is intimately connected with the search for superheavy nuclei [1, 2]. This is because spectroscopic information such as the energies of single-particle states and the rotational response can be used to constrain theoretical models and their parameterizations. The need for such a constraint is dictated by the fact that different theoretical models predict different locations for the “island of stability” of shell-stabilized superheavy nuclei. Macroscopic+microscopic methods based on different phenomenological potentials localize this island around the  $Z = 114$  and  $N = 184$  spherical shell closures [3, 4, 5]. Self-consistent calculations based on the Skyrme energy density functionals (EDF) show this island around the  $Z = 126$  and  $N = 184$  spherical shell closures for most of the forces [4, 6]. Covariant density functional theory (CDFT) [7] localizes this island around  $Z = 120$  and  $N = 172$  [2, 6].

Apart of the question of the location of the “island of stability”, the question of the stability of superheavy nuclei is another puzzle defining the physics of superheavy nuclei. The probability for the formation of a superheavy nucleus in a heavy-ion-fusion reaction and its survival are

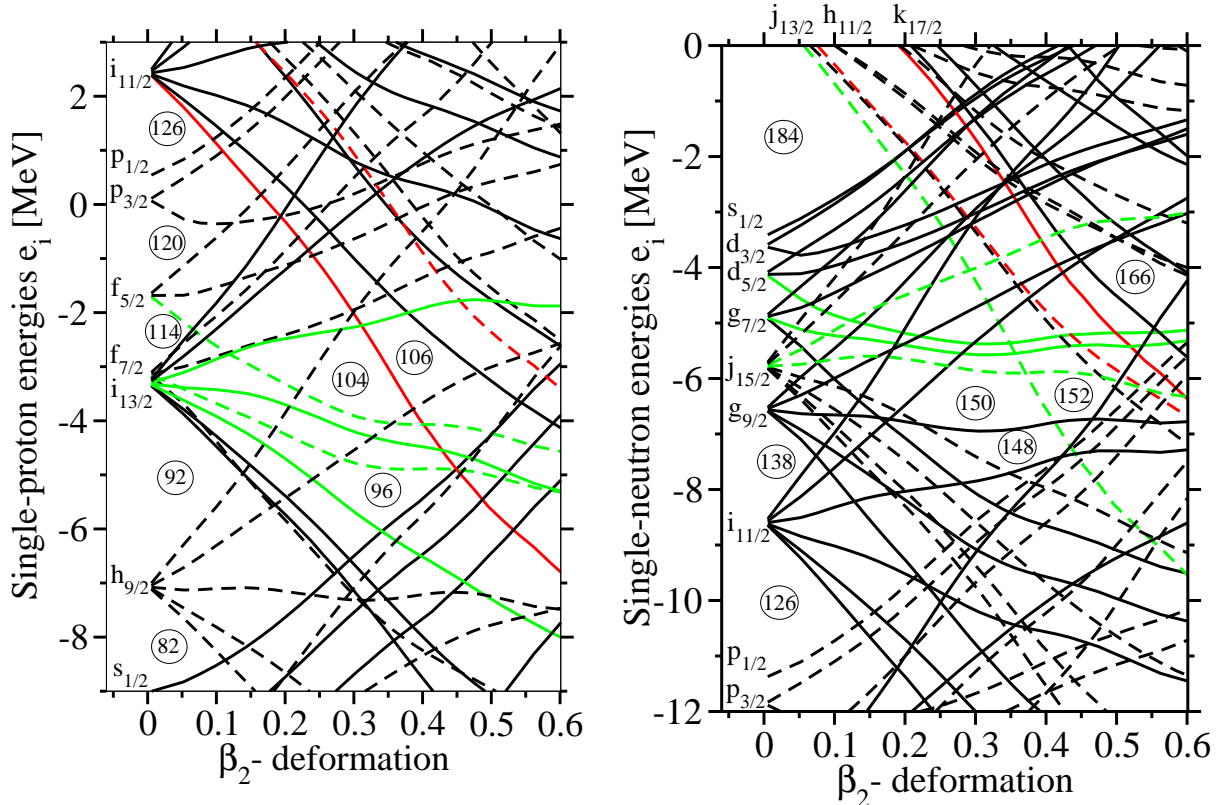


**Figure 1.** Proton and neutron single-particle energies in  $^{252}\text{No}$  as a function of the quadrupole deformation  $\beta_2$ . They are obtained in RMF+BCS calculations using the constant gap approximation and the NL1 parameterization of the RMF Lagrangian. Solid and dashed lines are used for positive and negative parity states, respectively. Green lines are used for the single-particle orbitals observed in odd-mass nuclei around  $^{250}\text{Fm}$ , while red lines are used for the  $\Omega = 1/2$  orbitals that may be observed in nuclides with  $N \approx 162$  and/or  $Z \approx 108$  [2].

directly connected to the height of its fission barrier [8]. Thus, the experimental data on fission barriers in the actinide region provide an important testing ground for density functional theories (DFT).

It is impossible to review all efforts undertaken in the study of theoretical aspects of the spectroscopy of the heaviest nuclei; thus we will concentrate on the results obtained in the framework of covariant density functional theory. The manuscript is organized in the following way. In Sec. 2, the accuracy of the description of the energies of deformed one-quasiparticle states in the actinide region and its consequences for spherical shell closures in superheavy nuclei are analyzed. The rotational response in odd-mass nuclei and its applicability for configuration assignment will be discussed in Sec. 3. The description of inner fission barriers in CDFT is discussed in Sec. 4. Finally, Sec. 5 summarizes our main conclusions.

## 2. Single-particle degrees of freedom

One way of obtaining information on the energies of spherical subshells active in the vicinity of expected shell closures in the “island of stability” is by studying well-deformed one-quasiparticle states in heavy actinide and/or light transfermium nuclei. As illustrated in the Nilsson diagram of Fig. 1, the deformation causes the spherical single-particle states to split and forces low- $\Omega$  states emerging from high- $j$  spherical subshells (for example, the  $\pi f_{5/2}$  and  $\pi i_{11/2}$  subshells, see

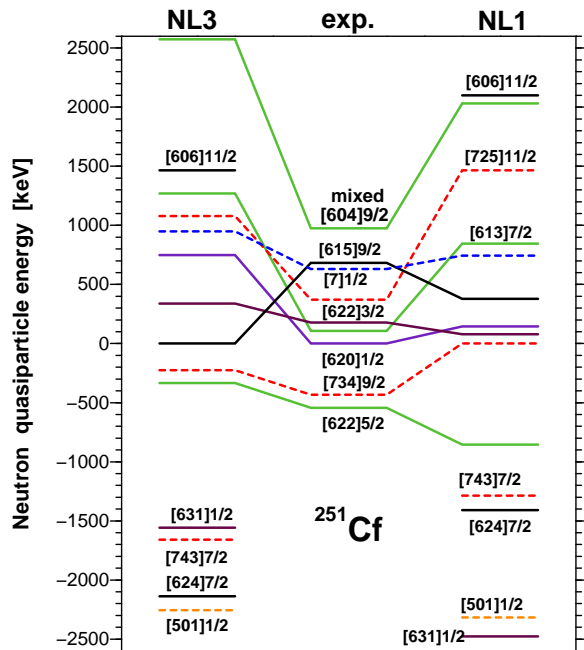


**Figure 2.** Experimental and theoretical one-quasiparticle energies of neutron states in  $^{251}\text{Cf}$ . Positive and negative energies are used for particle and hole states, respectively. The experimental data are taken from Refs. [9, 10, 11], while the results of calculations from Ref. [2]. Solid and dashed lines are used for positive and negative parity states, respectively. The symbols 'NL3' and 'NL1' indicate the RMF parameterization. Colors indicate the spherical subshells from which deformed one-quasiparticle states emerge, namely, green -  $2g_{9/2}$ , black -  $1i_{11/2}$ , indigo -  $3d_{5/2}$ , maroon -  $2g_{7/2}$ , red -  $1j_{15/2}$  and blue -  $1j_{13/2}$ .

left panel of Fig. 1) to come closer to the Fermi level in much lighter systems.

Nuclei around  $^{254}\text{No}$  represent the end of the region in which reliable experimental data on the structure of deformed one-quasiparticle states are available [1]. Although the decay studies of heavier odd-mass nuclei such as  $^{265}\text{Hs}$  and  $^{259}\text{Sg}$  (see, for example, Ref. [12] and references therein) probe one-quasiparticle states, these nuclei cannot be used for a meaningful comparison with theory because of the tentative nature of the configuration assignment. This is even more true for odd-mass nuclei with  $Z \geq 105$  which are identified by only a few events.

The first ever fully self-consistent description of deformed one-quasiparticle states in the framework of CDFT was presented in Ref. [2] on the example of the  $^{249,251}\text{Cf}$  and  $^{249}\text{Bk}$  nuclei. More systematic calculations covering the rare-earth and actinide regions and a number of the CDFT parameterizations are currently in progress [13]. Since these results confirm the general observations obtained in Ref. [2], we will illustrate the main features of the description of quasiparticle spectra of deformed nuclei on the example of  $^{251}\text{Cf}$  (see Fig. 2).

Two types of discrepancies between theory and experiment are visible in Fig. 2. *First, the calculated spectra are less dense than experimental ones.* This is especially visible in the pairs of deformed states emerging from the same spherical subshells (namely, the  $\nu 9/2[734]$  and  $\nu 11/2[725]$  states from the  $\nu 1j_{15/2}$  subshell as well as the  $\nu 5/2[622]$  and  $\nu 7/2[613]$  states from the  $\nu 2g_{9/2}$  subshell), the energy gaps between which are considerably stretched as compared with experiment. *Second, while the calculated energies of a number of states are rather close to experiment, the energies of some states and their relative positions deviate substantially from experiment.* For example, only NL1 gives the correct ground state  $\nu 1/2[620]$  in  $^{251}\text{Cf}$ , whereas NL3 gives the  $\nu[615]9/2$  (Fig. 2). The displacement of the calculated centroids of the above discussed pairs of deformed states from experimental ones clearly suggests that the discrepancies between experiment and calculations can be traced back to energies of spherical subshells from which deformed states emerge.

Comparing theory and experiment it was concluded in Ref. [2] that in the NL1 and NL3 parameterizations, the energies of the spherical subshells, from which the deformed states in the vicinity of the Fermi level of the  $A \sim 250$  nuclei emerge, are described with an accuracy better than 0.5 MeV for most of the subshells. The discrepancies (in the range of 0.6 – 1.0 MeV)

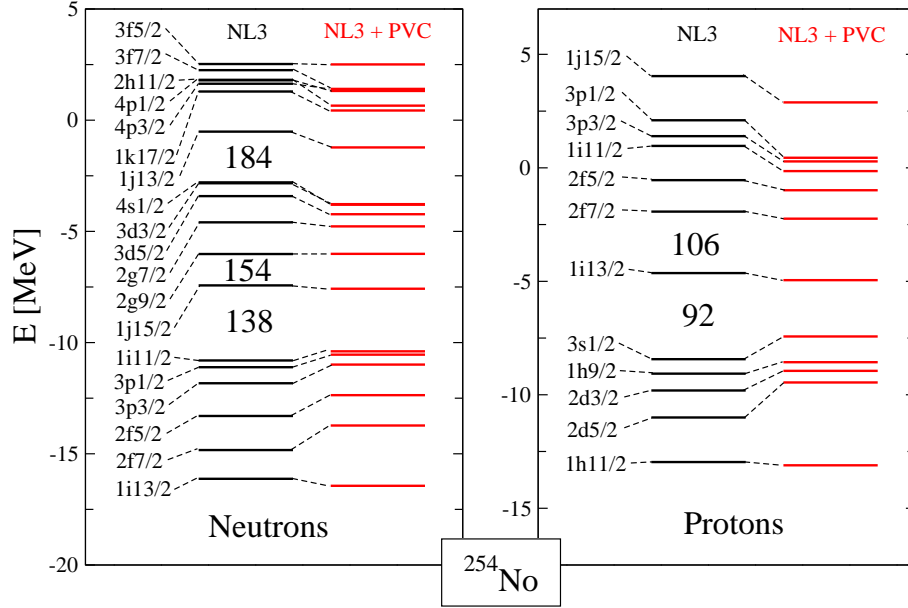


**Figure 3.** Neutron and proton single-particle states in  $^{254}\text{No}$  ( $Z = 102, N = 152$ ). The left column in each panel shows the spectra obtained in pure RMF calculations, while right column the spectra computed within RMF with allowance for the particle-vibration coupling. The calculations are performed at spherical shape employing the NL3 parameterization (from Ref. [14]).

are larger for the  $\pi 1h_{9/2}$  (NL3, NL1),  $\nu 1i_{11/2}$  (NL3),  $\nu 1j_{15/2}$  (NL1) and  $\nu 2g_{9/2}$  (NL3) spherical subshells. Considering that the RMF parameterizations were fitted only to bulk properties of spherical nuclei this level of agreement is good. In contrast, the accuracy of the description of single-particle states is unsatisfactory in the NLSH and NL-RA1 parameterizations. This clearly indicates that before extrapolating to superheavy nuclei the quality of the parameterization with respect of the description of single-particle energies has to be tested.

These results clearly indicate the need for an improvement in the description of the single-particle energies within CDFT. There are a number of possibilities which need further exploration. The stretching of the energy scale in CDFT calculations as compared with experiment is related to the low effective mass (Lorentz mass in the notation of Ref. [15])  $m^*(k_F)/m \approx 0.66$  of the nucleons at the Fermi surface in CDFT. It has been demonstrated for spherical nuclei that particle-vibration coupling brings the average level density in closer agreement with experiment in relativistic [16] and non-relativistic calculations [17]. This effect is clearly visible in Fig. 3 where the particle-vibration coupling leads to a pronounced increase of the level density around the Fermi surface both for proton and neutron subsystems comparatively to the pure RMF spectra. Similar effects are expected in deformed nuclei. However, the corrections to the energies of quasiparticle states in odd nuclei due to particle-vibration coupling are expected to be less state dependent in deformed nuclei because (due to fragmentation) the surface vibrations are less collective in deformed nuclei than in spherical ones [18].

The measured and calculated energies of the single-particle states at normal deformation provide constraints on the spherical shell gaps of superheavy nuclei. Such an analysis restricts the choice of CDFT parameterizations only to those which predict  $Z = 120$  and  $N = 172$  as shell closures in superheavy nuclei [2]. The inclusion of particle-vibration coupling compresses

the single-particle spectra in the ( $Z = 120, N = 172$ ) nucleus and decreases the size of above mentioned gaps. However, this nucleus still remains a doubly magic spherical superheavy nucleus in CDFT [14].

### 3. Rotational degrees of freedom

Additional information on the structure of single-particle states can be obtained by studying the rotational response in odd-mass nuclei. This is especially important for nuclei at the edge of the region where spectroscopic studies are possible (the nuclei with masses  $A \sim 255$ ), for which alternative methods of configuration assignment are not feasible. To illustrate that we use rotational structures in  $^{241}\text{Am}$ . The rotational bands based on the Nilsson orbitals  $\pi 5/2[642]$  (from the  $i_{13/2}$  subshell),  $\pi 5/2[523]$  (from the  $h_{9/2}$  subshell) and  $\pi 3/2[521]$  (from the  $f_{7/2}$  subshell) have been observed in this nucleus in Ref. [19]. As can be seen in the left panel of Fig. 4, at low frequencies they have distinctly different kinematic moments of inertia  $J^{(1)}$ . The theoretical interpretation of these bands has been performed in cranked relativistic Hartree+Bogoliubov (CRHB) theory [20, 2] employing the NL1 parameterization of the RMF Lagrangian and the D1S Gogny force in the pairing channel. In addition, approximate particle number projection has been carried out by means of the Lipkin-Nogami (LN) method. Theoretical calculations (right panel of Fig. 4) describe well the absolute values of the kinematic moment of inertia of different configurations and their evolution with rotational frequency. In particular, the splitting of two signatures of the  $\pi 5/2[642]$  configuration is rather well described in the model calculations. On the contrary, the  $\pi 5/2[523]$  and  $\pi 3/2[521]$  bands show (with exception of very low frequencies in the case of the  $\pi 3/2[521]$  band) no signature splitting. Model calculations for the two signatures of the  $\pi 5/2[523]$  configuration show explicitly this feature. Unfortunately, it was not possible to get convergence in the case of the  $\pi 3/2[521]^+{}^1$  configuration. However, the analysis of the quasiparticle routhian diagram confirms that the  $\pi 3/2[521]^\pm$  configurations have to be degenerate in energy up to rotational frequency  $\Omega_x \sim 0.16$  MeV in agreement with experimental observations. At higher frequencies, small signature separation is expected in the calculations.

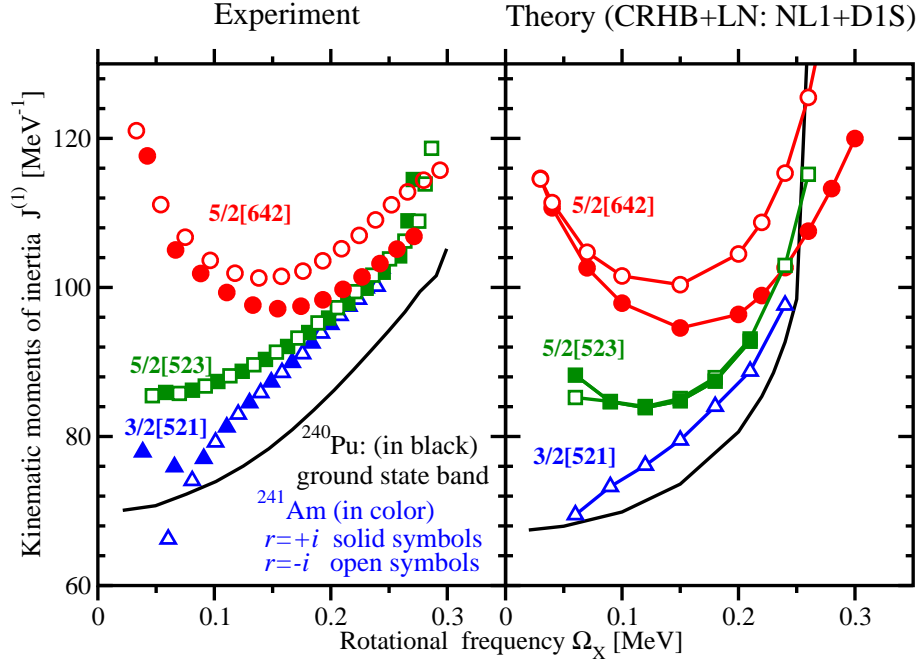
In addition to the above mentioned features, the relative properties of different bands both with respect of each other and with respect to  $^{240}\text{Pu}$  (which has one proton less) are well described in the model calculations. The increase of the kinematic moment of inertia in the bands of  $^{241}\text{Am}$  as compared with the ground state band in  $^{240}\text{Pu}$  is caused by the blocking effect which results in a decreased proton pairing.

Fig. 5 shows another example of the description of rotational bands in CRHB calculations. The single decoupled band observed recently in the odd-proton nucleus  $^{251}\text{Md}$  [22] has been assigned to the  $\pi 1/2[521]^-$  configuration. CRHB calculations have been performed for several low-lying configurations. However, the  $\pi 7/2[633]$ ,  $\pi 3/2[521]$ ,  $\pi 9/2[624]$  and  $\pi 9/2[505]$  configurations can be excluded from consideration because they lead either to signature degenerate bands or to bands with small signature splitting; as a consequence, both signatures are expected to be observed in experiment. On the other hand, the calculations for the  $\pi 1/2[521]^-$  configuration describe the experimental data rather well thus confirming the configuration assignment given in Ref. [22]. Note that the results obtained with the NL3 parameterization of the RMF Lagrangian are close to the ones obtained with NL1. Thus, they do not alter the interpretation of the observed band.

These two examples outline the current approach to the configuration assignment of one-quasiparticle states in odd-mass nuclei based on their rotational response. They clearly show that the rotational properties reflected through

- the absolute values of the kinematic moment of inertia (especially at low rotational

<sup>1</sup> The superscript to the orbital label is used to indicate the sign of the signature  $r$  for that orbital ( $r = \pm i$ ).



**Figure 4.** Experimental and calculated kinematic moments of inertia  $J^{(1)}$  of the indicated one-quasiproton configurations in  $^{241}\text{Am}$ . In addition, these moments are shown for the ground state band in  $^{240}\text{Pu}$ . Experimental data are taken from Refs. [19] ( $^{241}\text{Am}$ ) and [21] ( $^{240}\text{Pu}$ ).

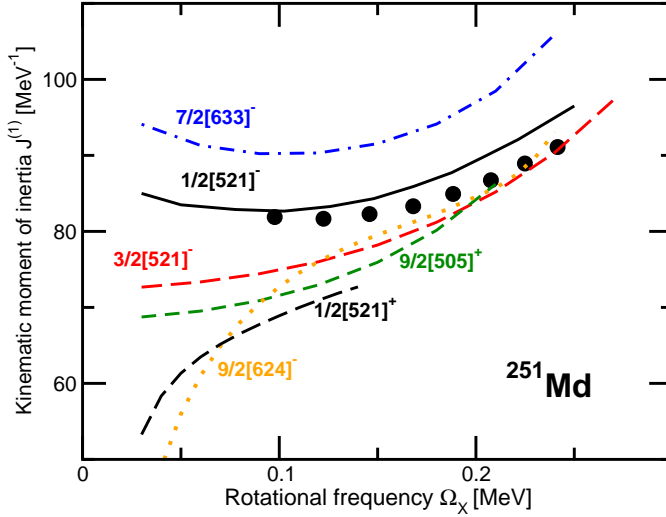


**Figure 5.** Calculated kinematic moments of inertia  $J^{(1)}$  of the indicated one-quasiproton configurations in  $^{251}\text{Md}$  are shown by lines. The configurations 7/2[633], 9/2[505], 9/2[624], 3/2[521] are either signature degenerate or characterized by small signature splitting. Thus, for simplicity we show the results only for one signature. The kinematic moments of inertia for observed band [22] are shown by solid circles.

frequencies) and their evolution with rotational frequency

- the presence or absence of signature splitting
- the relative properties of different configurations with respect of each other and/or with respect to the neighboring even-even nucleus

provide a useful tool for single-particle configuration assignment. However, it is necessary to recognize that this method of configuration assignment has to be complemented by other independent methods and has to rely on sufficient experimental data. The interpretation of the rotational band in  $^{253}\text{No}$  is quite illustrative in this respect. Initially, it was interpreted as based

on the  $\nu 7/2[624]$  configuration [23]. However, improved experiments allowed to identify the M1 transitions between opposite signatures of the observed band [23] which led to the  $\nu 9/2[734]$  configuration assignment. The kinematic moments of inertia of the observed band under two configuration assignments are described within a typical theoretical uncertainty<sup>2</sup>, and, as a result, the configuration assignment based only on rotational properties cannot be reliable. The branching ratios of observed M1 and E2 transitions have to be used in order to distinguish different configuration assignments [26].

#### 4. Fission barriers: the role of triaxiality

The (static) inner fission barriers  $B_f^{st}$  are important for several physical phenomena. The size of the fission barrier is a measure for the stability of a nucleus (which decays by spontaneous fission) reflected in its spontaneous fission lifetime [27]. The probability for the formation of a superheavy nucleus in a heavy-ion-fusion reaction is also directly connected to the height of its fission barrier [8]. The height  $B_f^{st}$  is a decisive quantity in the competition between neutron evaporation and fission of a compound nucleus in the process of its cooling [8]. The population and survival of hyperdeformed states at high spin also depends on the fission barriers [28, 29]. In addition, the  $r$ -process of stellar nucleosynthesis depends (among other quantities such as masses and  $\beta$ -decay rates) on the fission barriers of very neutron-rich nuclei [30, 31].

However, the progress in the study of the fission barriers within covariant density functional theory has been slower than in its non-relativistic counterparts [32]. Until now the majority of the calculations have been performed under the restriction to axial symmetry (see Ref. [32] and references therein). However, axially symmetric calculations cannot be directly compared with experimental data since, as has been shown earlier in non-relativistic calculations (see Refs. [33, 34] and references therein), the lowering of fission barriers due to triaxiality is significant and can reach 3 – 4 MeV in some nuclei. So far, the impact of triaxiality on the height of the inner fission barrier has only been studied in specific nuclei such as  $^{264}\text{Hs}$  [35] and  $^{240}\text{Pu}$  [36] within the RMF+BCS approach as well as  $^{240}\text{Pu}$  [37] within the RHB approach.

In order to fill this gap in our knowledge, a systematic investigation of the inner fission barriers within the triaxial RMF+BCS approach has been performed for the first time [38] employing the recently developed NL3\* parameterization [39] of the RMF Lagrangian. The truncation of the basis is performed in such a way that all states belonging to the shells up to  $N_F = 20$  fermionic shells and  $N_B = 20$  bosonic shells are taken into account. In the pairing channel, we use a seniority pairing force, with the strength parameters defined as in Ref. [38]:

$$A \cdot G_n = 9.1 - 6.4 \frac{N - Z}{A} \text{ MeV} \quad (1)$$

$$A \cdot G_p = 8.1 + 10.0 \frac{N - Z}{A} \text{ MeV} \quad (2)$$

Note that all states in the pairing window  $E_k < E_{\text{cutoff}} = 120$  MeV are taken into account. Because the nuclei considered are all well bound, pairing is treated in the BCS approximation.

The calculations are performed imposing constraints on the axial and triaxial mass quadrupole moments. The method of quadratic constraints uses a variation of the function

$$\langle H \rangle + \sum_{\mu=0,2} C_{2\mu} (\langle \hat{Q}_{2\mu} \rangle - q_{2\mu})^2 \quad (3)$$

<sup>2</sup> The calculations show that the kinematic moments of inertia in the nuclei of interest are described with an accuracy better than 10% of their absolute value, see current results and the results presented in Refs. [2, 24]. The only exception is the rotational band in  $^{255}\text{Lr}$ , where the discrepancy of around 15% is seen under the  $\pi[624]9/2$  configuration assignment [25]. On the basis of the moment of inertia, CRHB calculations favor the  $\pi 7/2[633]$  assignment. Note that the kinematic moments of inertia for the assigned  $\pi 7/2[633]$  and  $\pi 9/2[624]$  rotational bands in  $^{251}\text{Es}$  are described in CRHB calculations within 7% accuracy [25].

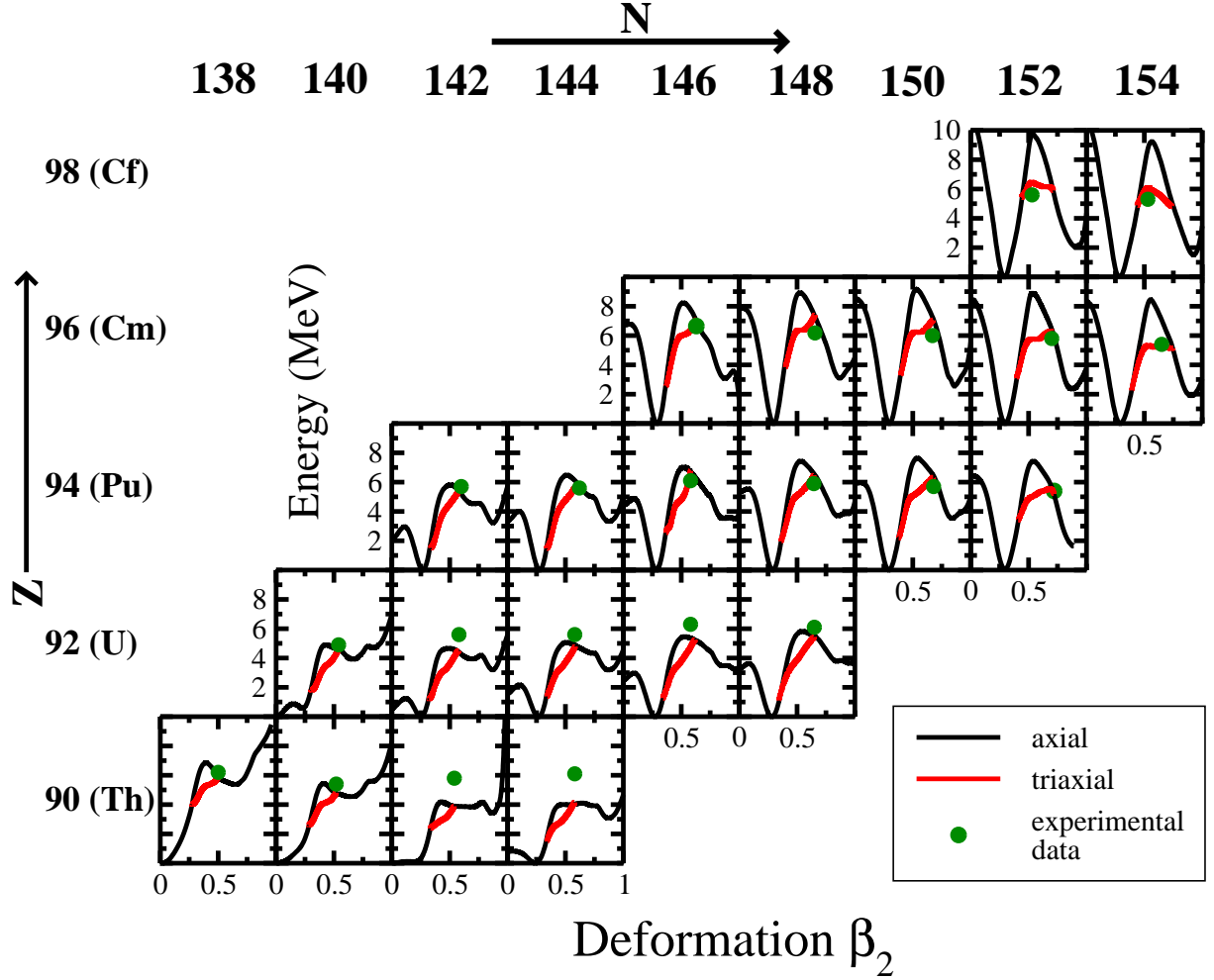


**Figure 6.** Deformation energy curves of even-even actinide nuclei obtained in RMF+BCS calculations with the NL3\* parameterization. Experimental data are taken from Table IV in Ref. [41]. A typical uncertainty in the experimental values, as suggested by the differences among various compilations, is of the order of  $\pm 0.5$  MeV [41]. See text for detail.

where  $\langle H \rangle$  is the total energy, and  $\langle \hat{Q}_{2\mu} \rangle$  denotes the expectation values of the mass quadrupole operators

$$\hat{Q}_{20} = 2z^2 - x^2 - y^2 \quad (4)$$

$$\hat{Q}_{22} = x^2 - y^2 \quad (5)$$

In these equations,  $q_{2\mu}$  is the constrained value of the multipole moment, and  $C_{2\mu}$  the corresponding stiffness constants [40].

The results of these systematic calculations are shown in Fig. 6. The deformation energy curves (shown by full black lines in Fig. 6) for axially symmetric solutions are obtained as the  $\gamma = 0^\circ$  cross-section of the potential energy surfaces. The deformation energy curves for triaxial solutions are obtained by the minimization of the potential energy surfaces along the  $\beta_2$ -direction. The deformation energy curves along the triaxial fission path are shown by red full curves. We show deformation energy curves for triaxial solutions only in the range of the  $\beta_2$  values at which it is lower in energy than the deformation energy curve of the axially symmetric



solution. Note that the potential energy surfaces are normalized to zero energy at the normal-deformed minimum. One can see that by allowing for triaxiality the fission barrier heights are reduced by 1 – 3 MeV as compared with axially symmetric solutions. This lowering depends on the proton and neutron numbers. It also brings on average the results of calculations in closer agreement with experimental data shown by green solid circles in Fig. 6. These circles display the height of the experimental fission barrier at the calculated  $\beta$ -deformation of the saddle point. On average calculated  $\gamma$ -deformations of the triaxial parts of the fission path are close to  $10^\circ$ .

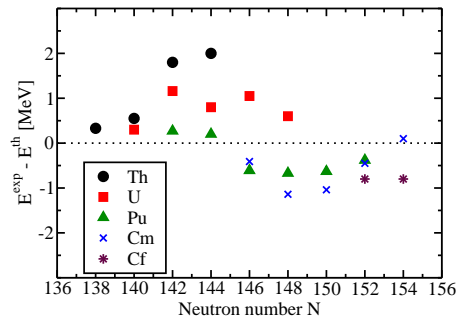


**Figure 7.** The difference between experimental and calculated heights of inner fission barriers as a function of neutron number  $N$ .

Fig. 7 shows the differences between calculated and experimental heights of inner fission barriers. The average deviation between theory and experiment is 0.76 MeV. This is comparable with the results obtained in the macroscopic+microscopic method (see Sec. IVC and Fig. 11 in Ref. [42] and Sec. VII A in Ref. [43]) which describe experimental fission barriers with an average error of around 1 MeV. It is necessary, however, to say that neither the proton nor the neutron particle number dependences of fission barrier height are completely reproduced in the calculations. This is exemplified in Fig. 7. However, the same problem exists also in macroscopic+microscopic calculations (see Fig. 11 in Ref. [42] and Figs. 23-32 in Ref. [43]). There are very few energy density functional calculations of the fission barriers which include triaxial deformations, and neither of them confronts in a systematic way experimental data in actinides. However, the limited results obtained with the Skyrme energy density functionals presented in Ref. [44] show similar unresolved particle number dependences for the inner fission barrier heights.

## 5. Conclusions

The analysis of quasiparticle spectra in actinides and heaviest  $A \sim 250$  nuclei provides a measure of the accuracy of the description of single-particle energies in CDFT. In addition, it restricts the choice of the CDFT parameterizations to only those which predict  $Z = 120$  and  $N = 172$  as shell closures in spherical superheavy nuclei. The inclusion of particle-vibration coupling does not change the position of shell closures for these nuclei.

The description of rotational properties in odd-mass nuclei within the framework of the cranked relativistic Hartree+Bogoliubov framework has been discussed. It is shown that rotational properties are reasonably well described. As a consequence, their theoretical analysis provides a useful supplementary tool in the assignment of single-particle configurations to rotational bands observed at the edge of the region where spectroscopic studies are possible.

The first systematic investigation of fission barriers in the actinide region with triaxiality accounted has been performed within covariant density functional theory. It is found that with only one exception ( $^{234}\text{Th}$ ) in all the nuclei under investigation the height of the inner fission barrier is reduced by allowing for triaxial deformations by 1 – 3 MeV. A systematic comparison of our results with experimentally determined fission barriers in this region shows reasonable agreement with data comparable with the best macroscopic+microscopic calculations.

## 6. Acknowledgments

This work has been supported by the U.S. Department of Energy under the grant DE-FG02-07ER41459 and by the DFG cluster of excellence “Origin and Structure of the Universe” (www.universe-cluster.de). E. L. is supported by the Hessian LOEWE initiative through the Helmholtz International Center for FAIR.

## References

- [1] Herzberg R D, Greenlees P T 2008 *Prog. Part. Nucl. Phys.* **61** 674
- [2] Afanasjev A V, Khoo T L, Frauendorf S, Lalazissis G A, Ahmad I 2003 *Phys. Rev.* **C67** 024309
- [3] Nilsson S G, Tsang C F, Sobiczewski A, Szymanski Z, Wycech S, Gustafsson C, Lamm I L, Möller P, Nilsson B 1969 *Nucl. Phys.* **A131** 1
- [4] Ćwiok S, Dobaczewski J, Heenen P H, Magierski P, Nazarewicz W 1996 *Nucl. Phys.* **A611** 211
- [5] Möller P, Nix J R 1994 *J. Phys.* **G20**, 1681
- [6] Bender M, Rutz K, Reinhard P G, Maruhn J A, Greiner W 1999 *Phys. Rev. C* **60** 034304
- [7] Vretenar D, Afanasjev A V, Lalazissis G A, Ring P 2005 *Phys. Rep.* **409** 101
- [8] Itkis M G, Oganessian Y T, Zagrebaev V I 2002 *Phys. Rev.* **C65** 044602
- [9] Ahmad I *et al* 2000 *Phys. Rev.* **C62** 064302
- [10] Ahmad I *et al* 1971 *Phys. Rev.* **C3** 390
- [11] Ahmad I, Chasman R R, Friedman A M, Yates S W 1990 *Phys. Lett.* **B251** 338
- [12] Heßberger F P *et al* 2009 *Eur. Phys. J.* **A41** 145
- [13] Shawaqfeh S, Afanasjev A, in preparation
- [14] Litvinova E, Afanasjev A V, in preparation
- [15] Jaminon M, Mahaux C 1989 *Phys. Rev.* **C40** 354
- [16] Litvinova E, Ring P 2006 *Phys. Rev.* **C73** 044328
- [17] Mahaux C, Bortignon P F, Broglia R A, Dasso C H 1985 *Phys. Rep.* **120** 1
- [18] Soloviev V G, *Theory of complex Nuclei* (Pergamon, New York, 1976)
- [19] Abu Saleem K *et al* 2004 *Phys. Rev. C* **70** 024310
- [20] Afanasjev A V, Ring P, König J 2000 *Nucl. Phys.* **A676** 196
- [21] Wang X *et al* 2009 *Phys. Rev. Lett.* **102** 122501
- [22] Chatillon A *et al* 2007 *Phys. Rev. Lett.* **98** 132503
- [23] Reiter P *et al* 2005 *Phys. Rev. Lett.* **95** 032501
- [24] Bastin J E *et al* 2006 *Phys. Rev.* **C73** 024308
- [25] Jeppesen H B *et al* 2009 *Phys. Rev. C* **80** 034324
- [26] Herzberg *et al* 2009 *Eur. Phys. J.* **A42** 333
- [27] Sobiczewski A, Pomorski K 2007 *Prog. Part. Nucl. Phys.* **58** 292
- [28] Dudek J, Pomorski K, Schunck N, Dubray N 2004 *Eur. Phys. J.* **A20** 15
- [29] Afanasjev A V, Abusara H 2008 *Phys. Rev.* **C78** 014315
- [30] Arnould M, Takahashi K, 1999 *Rep. Prog. Phys.* **62** 395
- [31] Mamdouh A, Pearson J M, Rayet M, Tondeur F, 2001 *Nucl. Phys.* **A679** 337
- [32] Karatzikos S, Afanasjev A V, Lalazissis G A, and Ring P 2010 *Phys. Lett.* **B689** 72
- [33] Warda M, Egido J L, Robledo L M, and Pomorski K 2002 *Phys. Rev.* **C66** 014310
- [34] Staszczak A, Baran A, Dobaczewski J, and Nazarewicz W 2009 *Phys. Rev.* **C80** 014309
- [35] Bender M, Rutz K, Reinhard P G, Maruhn J A, Greiner W 1998 *Phys. Rev.* **C58** 2126
- [36] Bender M, Heenen P H, and Reinhard P G 2003 *Rev. Mod. Phys.* **75** 121
- [37] Li Z P, Nikšić T, Vretenar D, Ring P, Meng J 2010 *Phys. Rev.* **C81** 064321
- [38] Abusara H, Afanasjev A V, Ring P 2010 submitted to *Phys. Rev. C*
- [39] Lalazissis G A, Karatzikos S, Fossion R, Peña Arteaga D, Afanasjev A V, Ring P 2009 *Phys. Lett.* **B671** 36
- [40] Ring P, Schuck P, *The Nuclear Many-Body Problem* (Springer-Verlag, Berlin, 1980).
- [41] Samyn M, Goriely S, Pearson J M 2005 *Phys. Rev. C* **72** 044316
- [42] Dobrowolski J, Pomorski K, Bartel J 2007 *Phys. Rev.* **C75** 024613
- [43] Möller P, Sierk A J, Ichikawa T, Iwamoto A, Bengtsson R, Uhrenholt H, Åberg S 2009 *Phys. Rev.* **C79** 064304
- [44] Bonneau L, Quentin P, Samsen D 2004 *Eur. Phys. J.* **A21** 391